Published in final edited form as:

Cell Calcium. 2012 August ; 52(2): 152–160. doi:10.1016/j.ceca.2012.04.018.

Multi-Scale Data-Driven Modeling and Observation of Calcium Puffs

Ghanim Ullah[a], **Ian Parker**[b], **Don-On Daniel Mak**[c], and **John E Pearson**[a,*]

[a]Theoretical Biology and Biophysics, Los Alamos National Laboratory, Los Alamos, New Mexico

[b]Departments of Neurobiology and Behavior, Physiology and Biophysics, University of California, Irvine, California

[c]Department of Physiology, University of Pennsylvania, Philadelphia, Pennsylvania

Abstract

The spatiotemporal dynamics of elementary Ca^{2+} release events, such as “blips” and “puffs” shapes the hierarchal Ca^{2+} signaling in many cell types. Despite being the building blocks of Ca^{2+} patterning, the mechanism responsible for the observed properties of puffs, especially their termination is incompletely understood. In this paper, we employ a data-driven approach to gain insights into the complex dynamics of blips and puffs. We use a model of inositol 1,4,5-trisphosphate (IP_3) receptor (IP_3R) derived directly from single channel patch clamp data taken at 10μM concentration of IP_3 to simulate calcium puffs. We first reproduce recent observations regarding puffs and blips and then investigate the mechanism of puff termination. Our model suggests that during a puff, IP_3Rs proceed around a loop through kinetic states from “rest” to “open” to “inhibited” and back to “rest”. A puff terminates because of self-inhibition. Based on our simulations, we rule out the endoplasmic reticulum (**ER**) Ca^{2+} depletion as a possible cause for puff termination. The data-driven approach also enables us to estimate the current through a single IP_3R and the peak Ca^{2+} concentration near the channel pore.

Keywords

ion channel; IP_3R; puffs; blips; Ca^{2+} signaling; puff termination

1 Introduction

Calcium (Ca^{2+}) is a highly specific universal second messenger. The means by which a single ion can be both highly specific and universal is believed to lie in its spatiotemporal dynamics which are mediated by ion channels, pumps, and Ca^{2+} buffers [1]. One of the more intriguing aspects of the Ca^{2+} signaling toolkit are puffs which are brief (~ few tens of milliseconds) releases of Ca^{2+} through IP_3Rs from the **ER** store. The IP_3Rs are believed to be distributed in clusters [2-4]. Puffs result from the coordinated activity of multiple IP_3Rs in the cluster [5-7]. Ca^{2+} puffs and blips (Ca^{2+} release events due to single open IP_3R) are the building blocks of the increasingly complex spatiotemporal Ca^{2+} signaling patterns observed in several cell lines. Thus it has proved necessary to build models that can explain

---

[*]Corresponding Author: John E. Pearson, Theoretical Biology and Biophyiscs, T-10 (Base 6), P O Box 1663, MS K710, Los Alamos National Laboratory, Los Alamos NM 87545, pearson@lanl.gov, Tel: (505) 667-7585.

puff data [8-16]. Despite all these valuable efforts, certain aspects of puff dynamics such as their termination, remain incompletely understood. The goal of this work is to use a data-driven approach to; (1) reproduce recent observations about Ca^{2+} puffs, (2) investigate the mechanism of puff termination, and (3) give a reasonable estimate for the current through single IP_3R and the maximum Ca^{2+} concentration near the channel pore.

Recently one of us (Parker) reported observations in which the change in a Ca^{2+} fluorescent indicator in SH-SY5Y cells that are thought to reflect the openings or closings of individual channels is observed [5, 17]. By measuring the step changes in fluorescence that reflect openings or closings of individual channels during a Ca^{2+} puff, we found that at most 10-20 channels are simultaneously open. More often, about 6-10 channels open simultaneously. In this paper, we assume that the maximum amplitude (or number of simultaneously open channels) ever observed at a given puff site represents the number of channels within the cluster. Experimental observations suggest a typical cluster diameter of 0.3 – 0.8 μm [2, 5, 18]. This implies that the mean distance between nearest neighbor channels is about 100 – 150 nm depending on the size and number of channels within a cluster. Previous studies concluded that a single IP_3R channel releases a current I of about 0.025 – 0.5 pA [18-20]. Throughout this paper we will use a standard single-channel current of 0.075 pA. Based on the comparison between the model results and puff observations, we will argue that this is a reasonable value for the single channel current.

The IP_3R is a Ca^{2+}- sensitive Ca^{2+} channel. Single-channel measurements reveal that the equilibrium open probability (P_O) of IP_3R is bell-shaped with respect to Ca^{2+} [21, 22]. It is more probable for the channel to be open in the presence of 2 μM Ca^{2+} on the cytosolic side of the membrane than it is for it to open at 0.1 μM Ca^{2+} or 100 μM Ca^{2+}. We use this property of IP_3R along with kinetic data from the ligand concentration jump experiments [23] to develop a model for single-channel gating on which we build our puff model. Although several models for IP_3R exist in literature (e.g. [22, 24, 25]), it seems more appropriate to use a data-driven single channel model for puff simulation in order to better assess our predictions.

We construct a model for puffs based on fairly coarse properties of the IP_3R. The properties that we base our model on are (i) a simplified four-state Markov chain for the single-channel gating kinetics that we will argue is relevant to gating during puffs, (ii) the presumptive spatial distribution of channels, and (iii) the diffusion of Ca^{2+} from channel to channel in the presence of buffers. The model can account for the gross features of Ca^{2+} puffs with a single set of parameters. The model indicates that channels open because of cross-activation (in which channel A releases Ca^{2+} which then diffuses and causes nearest-neighboring channel B to experience near optimal $Ca^{2+} \approx 2\ \mu M$). The model further indicates that puffs terminate because of self-inhibition (in which channel A becomes inhibited after sensing high $Ca^{2+} > 100\ \mu M$ near its own channel pore). We rule out the possibility of **ER** depletion as the reason for puff termination. With the mean transition times between various states of the IP_3R constrained by the patch-clamp data and other parameters for Ca^{2+} and buffers kinetics available in the literature, we constrain the single channel current and Ca^{2+} concentration near the channel pore based on model comparison with the puffs data.

2 Single Channel Model

The gating of IP_3R depends on both Ca^{2+} (C) and IP_3 (I) concentrations. First, we will develop a seven state model that explains both the C and I dependence of the P_O of a single IP_3R channel. Once we have the seven state model, we will determine a simple four state model that reproduces the IP_3R P_O at fixed $I = 10 \mu M$ with the same accuracy as the full seven state model. We will build our puff model on the four state model.

The derivation of seven state model that explicitly treats IP_3 binding is shown in Supplemental Methods section 1.1. The scheme for the seven state model is shown in Fig. 1S and the model fit to the P_O of IP_3R in *Xenopus laevis* oocytes is shown by the lines in Fig. 2S.

Next we will derive the four state model that explains the gating of IP_3R under fixed $I = 10\mu M$ and varying C. The P_O of IP_3R as a function of C at fixed $I = 10\mu M$ is shown by the circles in Fig. 1. Each circle in Fig. 1 is the mean of multiple patch clamp experiments at given C value and the error bars are the standard errors of the mean. Using the information criterion [26] in the same manner as done for the seven state model, we find that the best fit to the P_O data at $I = 10\mu M$ is obtained by using the following function in C only. Note that the “best fit” here refers to the fit to the P_O data at fixed $I = 10\mu M$ and varying C unlike the seven state model that involves both Ca^{2+} and IP_3 dependence.

$$P_O = \frac{K_O C^2}{Z} \quad (1)$$

$$Z = 1 + (K_A + K_O)C^2 + K_I C^5. \quad (2)$$

Similar to the constant $K_{X_{ij}}$ in case of seven state model, the constants K_A, K_O, and K_I will be associated with forward equilibrium constants below. To simplify the notation, we have dropped the indices ij representing the number of Ca^{2+} and IP_3 bound to the channel. The fit to the P_O data at fixed $I = 10\mu M$ given by equation (1) is shown with solid line in Fig. 1. Like the seven state model, at least one state can be associated with each distinct monomial in the P_O. The monomials here are: 1, K_AC^2, K_OC^2, and K_IC^5. Thus we have four states: **R, A, O**, and **I**. 1, K_AC^2, K_OC^2, and K_IC^5 in Z are the occupancies of **R, A, O**, and **I** states respectively with respect to **R** state. As will become clear below, in each state, the channel has four IP_3 molecules bound. So, the occupancy of each state is multiplied by I^4, where I is the IP_3 concentration. For example, the occupancy of **A** state is $K_AC^2I^4$ etc. However, I^4 cancels out from the P_O equation.

The equilibrium occupancies of **R, A**, and **I** states are given by:

$$P_R = \frac{1}{Z} \quad (3)$$

$$P_A = \frac{1}{Z}\left(\frac{C}{C_A}\right)^2 \quad (4)$$

$$P_I = \frac{1}{Z}\left(\frac{C}{C_I}\right)^5 \quad (5)$$

The constants $K_A = \left(\frac{1}{C_A}\right)^2$, $K_O = \left(\frac{1}{C_O}\right)^2$, and $K_I = \left(\frac{1}{C_I}\right)^5$ are products of forward equilibrium constants along any path connecting the R state to the A, O, and I states respectively.

Thus we represent a single IP_3R by a four-state model shown in Fig. 2. The model is consistent with the single-channel kinetics under conditions of $10\mu M$ IP_3 concentration and with rapid perfusion experiments [23]. The four state model has a *rest* state (**R**) with no Ca^{2+} ions bound, an *active* closed state (**A**) with 2 Ca^{2+} bound, an *open* state (**O**) with 2 Ca^{2+}

bound, and an *inhibited* state (**I**) with 5 Ca^{2+} bound. We take 5 Ca^{2+} to be bound in the inhibited state as that provides the best fit for the P_O observed in *Xenopus laevis* oocytes. Under optimal[1] conditions ($C = 2\mu M$ and $I = 10\mu M$) the most probable behavior of the channel is that it flickers on and off between the open and active closed states. Our analysis indicates that 4 is the minimum number of states with four IP_3 molecules bound to the receptor in order to account for the equilibrium P_O of IP_3R channels under 10μM IP_3. We calculate the mean transition times from the P_O data obtained from *Xenopus laevis* oocytes and rapid perfusion experiments [23] as described below.

Comparison of the four state model to the seven state model reveals that states R, A, O, and I in the four state model are the same as the four states in the top loop of the seven state model where they are represented by R04, A24, O24, and I54. Thus the IP_3 dependence adds three more states (R00, A20, and I50) to the model. It is worth noticing that for the seven state model we took R00 as the reference state (hence $K_{R00} = 1$) while for the four state model we take R (represented by R04 in the seven state model) as the reference state. That is why we get different values for the occupancies of states R04, A24, O24, and I54 as compared to R, A, O, and I in the four state model. If we take R04 as the reference state, the occupancies of four states in the top loop of the seven state model are almost the same as the occupancies in the four state model. For the seven state model, the occupancy of state A24 relative to R04 = $K_{A24}\, C^2\, I^4/K_{R04}\, I^4 = (C/C_{A24})^2$ where $C_{A24} = (K_{R04}/K_{A24})^{1/2} = 0.52\mu M$. The occupancy of state O24 relative to R04 = $K_{O24}C^2I^4/K_{R04}I^4 = (C/C_{O24})^2$, $C_{O24} = (K_{R04}/K_{O24})^{1/2} = 0.26\mu M$. Similarly, the occupancy of I54 state relative to R04 = $K_{I54}\, C^5\, I^4/K_{R04}\, I^4 = (C/C_{I54})^5$, $C_{I54} = (K_{R04}/K_{I54})^{1/5} = 6.7\mu M$. C_{A24}, C_{O24}, and C_{I54} in the seven state model have the same meanings as C_A, C_O, and C_I in the four state model respectively. The values obtained here for the seven state model are very close to those for the four state model (Table 2S).

As clear from Fig. 2S, the P_O at $10\mu M$ IP_3 concentration given by the seven state model is exactly the same as given by the four state model. Thus for the remaining of this paper we will use the four state model to explore the behavior of puffs as both models behave in the same manner under $10\mu M$ IP_3 concentration.

In principle the network can be learned completely from the ligand-dependent steady state dwell–time distributions but we have not yet done that. Rather, we turn to some of the coarser features of kinetic data that we have reported previously [23].

The kinetic data suggests that there is a direct link between **O** and **I** and that there is no direct link between **R** and **O**. We performed kinetic measurements on Sf9 cells [23] in which we measured the response of the channel to rapid jumps in the concentrations of both IP_3 and Ca^{2+}. The distribution of "inhibition latencies" $f_i(t_i)$ (the distribution of times for the channel to go from actively gating to inhibited) is of particular interest. To measure the inhibition latency we jumped C from optimal ($C \approx 2\mu M$ where the P_O is maximal or near maximal) to inhibiting ($C \approx 300\mu M$ where P_O is near zero) at fixed IP_3 concentration of 10 μM. If the channel had needed to traverse some sequence of states to get from the open state to the inhibited state (or states) there would have been no short inhibition latencies: $f_i(0)$ would have been zero or near zero. At least with the resolution afforded by our experiments there appear to be no states intermediate to **O** and **I**. We therefore conclude that the open state is directly connected to the inhibited state. Similarly the distribution of times to recover from inhibition (after dropping C from 300 μM to 2 μM), $f_{ir}(t_{ir})$, is nonzero at $t_{ir} = 0$ which is further evidence in support of a direct link between **O** and **I**. In the case of *Xenopus laevis* oocytes it seems unlikely that the doubly liganded open state is directly connected to the

---

[1] We use the term "optimal" loosely to indicate a condition under which the IP_3R has a fairly high P_O.

inhibited state which has 5 Ca^{2+} bound but the intermediate states have low occupancy. We have not performed kinetic measurements on *Xenopus* but we believe that the connectivity will be similar to that of the Sf9 cells. We believe that any states that are intermediate to the open and the inhibited states are traversed so rapidly that transition times as short as $0.1 ms$ should be common. There appears to be nothing in the data that demands a link between **A** and **I**. We did report a deficit of short activation latencies when we jumped C from $< 10 nM$ to optimal. This implies that **R** is not directly connected to **O**. In another set of experiments, we jumped C from near 0 ($C < 10$ nM) to inhibiting value of 300 μM and found that 9 out of 103 experiments failed to cause channel bursts. Similarly, in experiments where we jumped C from 300 μM to < 10 nM, 88 out of 94 times the channel deactivated without bursting. Both these observations suggest a direct link between **R** and **I** states.

Thus the kinetic data for the *Xenopus Leavis* cell appears to be consistent with a network topology shown in Fig. 2. Note that we are interested in making a quantitive comparison to the puffs observed in SH-SY5Y cells. There are no single channel data available on the IP_3R kinetics in SH-SY5Y cells. We assume that the network topology is consistent with the network illustrated in Fig. 2.

The only states we are including here have 0, 2, 2, and 5 Ca^{2+} bound. Clearly there is a “missing state” with one Ca^{2+} bound that mediates the transition between the rest state **R** which has no Ca^{2+} bound, and the active state **A**, which has two Ca^{2+} bound. We denote this missing low occupancy state by $\mathbf{A}_1$. Similarly, there are two low occupancy states between **O** and **I** and 4 low-occupancy states between **I** and **R**. The P_O data are not adequate to provide accurate estimates of the occupancy of these states save that their occupancy is always low relative to that of the four primary states: **R, A, O, I**. Note that this does not imply that the occupancy of $\mathbf{A}_1$ is less than the occupancy of **R** for all C. Rather, it means that the occupancy of $\mathbf{A}_1$ is negligible compared to at least one of the four main states. Applying Occam’s razor, we set the occupancy of all the required low occupancy transition states to zero. Although these states have low occupancy, they impact the kinetic behaviors of the channel, serving as “speed bumps” for the probability flux between high occupancy states. The occupancy of transition states is low because the rates out of these states are high and this results in a finite probability flux. We introduce constants k_{ij}^{flux} which we call “flux parameters” because they give the equilibrium probability flux between states. For example, $k_{12}^{flux}C^2$ is the flux of probability from $\mathbf{A}_1$ which has one Ca^{2+} ion bound to **A** which has two Ca^{2+} ions bound. We present the explicit derivation of the mean times between the four primary states under the assumption that they are separated by low occupancy transition states in Supplemental Methods sections 1.2 and 1.3. The transition rates are the inverses of the mean transition times.

3 Stochastic Simulations of the IP_3R Cluster and Diffusion of Cytosolic Ca^{2+} and Buffers

We consider a cluster of 10 IP_3R channels arranged in a two dimensional array with an inter-channel spacing of 120 nm. The gating of each channel is given by the four state model described in the previous section. Details of the stochastic scheme and diffusion of Ca^{2+} and buffers are given in Supplemental Methods sections 1.4 and 1.5 respectively.

Our evolution equations (Eqs. 37S-40S) neglect the consumption of buffers in the vicinity of the j^{th} channel due to Ca^{2+} released by the i^{th} channel (with $i \neq j$) as the buffer consumed by a channel near its own pore is much higher than the buffer consumed by the same channel at the location of its neighbor. This would be an exact approximation if the channels were infinitely apart. The fact that channels in the cluster are at finite distance from each other makes this a crude approximation but not as crude as others made in the field [12, 27, 28]. The propagation of Ca^{2+} and buffers is simulated throughout a 3D cytosolic space. Considering the spherical symmetry around the channel, the Laplacian of Ca^{2+} and buffers in spherical coordinates is given as

$$\nabla_j^2 X(r_j, t) = \frac{1}{r_j^2}\frac{\partial}{\partial r_j}\left(r_j^2 \frac{\partial X}{\partial r_j}\right) \quad (6)$$

where $X = c, b_m, b_d$.

We solve the set of differential equations (Eqs. 37S-40S) *implicitly* on a hemispherical volume of radius 5 μm with a spatial grid size of 5 nm for each channel and sum the contribution of all channels for the instantaneous Ca^{2+} concentration at a given point in space. The idea is that we are simulating the dynamics of a puff-site that is far from the plasma membrane, in essence a single puff-site in a semi-infinite medium. Under the simulated conditions the Ca^{2+} concentration at 5 μm does not change significantly. Thus we use 5 μm as the radius of the simulated volume. Increasing the radius of the simulated volume does not make an appreciable difference. The assumption that each channel has its own reservoir of buffers converts the 3D problem into N 1D problems, where N is the total number of channels. In this case, we solve 10 1D problems each with 1000 grid points. Solving this problem numerically with similar resolution in cartesian coordinates, for example, would require about a billion grid points, a very demanding computational job where thousands of puffs have to be simulated to extract statistics. The details of computational scheme are given in Supplemental Methods section 1.6.

Finally, Ca^{2+} concentration at the location of each channel is updated by adding the contributions from other channels in the cluster

$$C_i = \sum_{j=1}^{10} c^j(r_{ij}) \quad (7)$$

Where r_{ji} is the distance between channels i and j, and c^j is the Ca^{2+} concentration at a given point in space and time due to channel j.

This method is similar in spirit to the quasi-static approximation made by Nguyen, et al. [27] where local Ca^{2+} experienced by channel i due to other channels was calculated as $C_i = \sum_{j=1}^{N} \frac{I_j e^{-r/\lambda}}{2\pi D r}$. Here I_j, r, λ, and D is the source amplitude of channel j, distance of channel j from channel i, buffer space constant, and effective diffusion coefficient of Ca^{2+} respectively. $I_j = 0$ when the channel j is closed (see also [28]). The approximation made by [27, 28] is binary; an open channel contributes $\frac{Ie^{-r/\lambda}}{2\pi D r}$ while a closed channel makes no contribution to the overall Ca^{2+} profile. We relax the binary static approximation made in these two studies. When a channel first opens the contribution to the overall Ca^{2+} profile is approximately $\frac{Ie^{-r/\lambda}}{2\pi D r}$. The contribution to the profile continues to evolve on a slow time-scale. When an open channel first closes, its contribution to the overall profile rapidly drops to a low but nonzero level and then decays slowly to zero. Furthermore, when the first channel opens, the quasi-static approximation made by Nguyen et al [27] fixes the first channel's contribution to the Ca^{2+} concentration at the second channel. In reality, the first channel's contribution to the Ca^{2+} concentration at the second channel will continue to increase as long as the first channel is open. Our approximation tracks these time-dependent contributions of the channels to the Ca^{2+} profile.

We estimate the fluorescence signal from total internal reflection fluorescence (TIRF) microscopy by the procedure outlined in [19] which is described in Supplemental Methods section 1.7. Details of experimental protocol are given in Supplemental Methods section 1.8.

4 Results

4.1 Puffs Statistics

The stochastic scheme described above allowed us to simulate Ca^{2+} puffs produced by a single cluster of 10 IP_3Rs and blips due to a single channel inside the cluster. The simulation results are shown in Figs. 3, 4. Fig. 3 shows a representative time series of random Ca^{2+} puffs caused by cooperative openings of multiple channels. The modeled fluorescence changes in response to channel openings and closings in units of average fluorescence change during blips are shown in panel (A). That is, we measured the fluorescence changes during thousands of blips and used the average of these measurements as a unit for fluorescence changes during puffs and blips. The corresponding number of open channels during puffs and blips are shown in panel (B). One can clearly see step level changes in the fluorescence in response to channel openings and closings. The time series also show examples of Ca^{2+} blips caused by single channel openings (Fig. 3B). An expanded view of a single puff reveals that the changes in fluorescence are slower than the time-scale in which the channels open and close (insets in Fig. 3A, B). In the example shown in the insets, there is a single-channel event right before the puff in the open channels trace that cannot be detected in the fluorescence trace. Thus it is not possible to detect very brief channel openings and closings during the puff from fluorescence measurements. Furthermore, the amplitude of the fluorescence does not necessarily represent the actual number of open channels. In the insets, the numbers 1 and 2 correspond to four and three open channels, respectively (Fig. 3B inset). However, in the fluorescence, the peak corresponding to four open channels (1 in the inset) is lower than that corresponding to three open channels (2 in the inset) because three channels were open longer. This point will be further elaborated in Fig. 5 below. The distribution of all peak and step level amplitudes obtained from the simulated fluorescence data (see Fig. 3 for examples) is shown in Fig. 4 in units of blip amplitude. That is, we detected all step level changes in fluorescence due to channel openings and quantified them in unit of averaged fluorescence change during a blip. Peaks at integral values of amplitude similar to those from experimental observations can be clearly discerned (Fig. 4A of [5]).

The distributions of various statistical properties calculated for several thousand puffs and blips are shown in Fig. 5. The distribution of puff amplitudes (maximum number of open channels during a puff) compares reasonably well with the experimental data from SH-SY5Y cells shown by the gray bars (Fig. 5A). The experimental data is modified from [5] by considering the puffs with maximum number of channels ≤ 10 and computing the distribution over this range in order to be consistent with a cluster size of 10 channels. Fig. 5A clearly shows that there are significant differences in the amplitude distributions obtained from modeled fluorescence and open channel count. The distribution obtained from modeled open channel counts has more small events and fewer big events compared to the distribution obtained from modeled fluorescence. As we will discuss below, the discrepancy between the distributions from modeled fluorescence and experiment decreases as we increase the transition rates between states **O** and **I**.

The distribution of puff life-times is shown in Fig. 5B. Our simulation generates puffs with shorter durations than earlier experimental observations [7]. However, the new improved imaging technique reveal shorter puff durations [5]. Furthermore, as we will show below the durations of puffs estimated from fluorescence measurements can be slightly longer than those estimated from the number of open channels.

The puff termination time (time from the peak of the puff to the base-line Ca^{2+}) follows an exponential decay with a peak around 40 *ms* for the distribution obtained from the open channel count which is the same as the peak of distribution from TIRF experiments (Fig. 5C). All the distributions in Fig. 5C are based on puffs with 5 to 10 open channels. The distribution obtained from modeled fluorescence peaks around 70 *ms*. The distribution of puff termination time obtained from modeled fluorescence is shifted to the right when compared to the distribution from open channel count. This result indicates that the puffs actually have shorter termination time and duration than that estimated by fluorescence microscopy. We will discuss the discrepancy between the distributions from the model and experiment below.

The model is in good agreement with the distribution of Ca^{2+} blip life-times from single-channel events (Fig. 5D).

The modeled mean time to puff termination as a function of puff amplitude estimated from both the number of open channels and fluorescence is shown in Fig. 5E. The mean termination time versus amplitude of the puff estimated from number of open channels (solid line with open squares) is well in the range of experimentally observed values (light gray bullets). While the mean termination time estimated from modeled fluorescence (solid line with filled squares) shows longer puffs consistent with Fig. 5C. The mean termination time versus amplitude nearly follows a harmonic series as shown by the dashed line. We will discuss the significance of this behavior in the final section.

Fig. 5F shows the rate of channel openings (upper panel) and closings (lower panel) per puff as a function of time after puff initiation. The rate of channel openings and closings were calculated by counting the total number of channels that opened or closed during consecutive time windows of 5 *ms* and averaging the result over all puffs for that time window. For example, the average openings during the time 0 – 5 *ms* is calculated by counting the total number of channels that opened during the first 5*ms* of each individual puff and then averaging the result for all puffs. Finally, the average was divided by 5 *ms*. The open rate drops from high to low value rapidly in the initial phase of the puff. Channel opening and closing rates both agree with experimentally observed values (gray bullets in Fig. 5F). For the simulation shown in Fig. 5, the average statistics of puffs are: amplitude, 3.57 channels; duration, 37.40 *ms*; openings/ms, 0.44; closings/ms, 0.49; frequency 0.46puffs/sec; and duration of blips, 10 *ms*. Interestingly, we find that the stationary buffer and EGTA do not significantly effect the statistics of elementary Ca^{2+} release events (Fig. 3S).

The major discrepancy of our model is its prediction of longer termination time for bigger puffs as compared to the experimental data (Fig. 5C, E). There are two possible explanations for this discrepancy. First, the experimental distribution in Fig. 5C is based only on those puffs with no channel re-openings during the falling phase. That is, puffs where channels re-opened during the termination phase were not considered in the analysis. The second source of discrepancy comes from the mean times for the transitions between O and I states. As we will discuss further in the final section, the higher number of channel re-openings during the falling phase of the puff is the major contributor to the longer puff termination time. The number of re-openings decreases as we increase the transition rates between O and I states. We estimated the transition rates from the ligand jump experiments performed on IP_3R in Sf9 cells [23]. It is possible that the mean transition times between O and I states of IP_3R in

SH-SY5Y cells are shorter than that for IP_3R in Sf9 cells, thereby giving rise to higher transition rates between states O and I. Indeed, the termination time for bigger puffs decreases as we decrease the mean time for the transitions between O and I states (Fig. 5E, dotted line with triangles), shifting the termination time distribution to the left (Fig. 5C, dotted line). Decreasing the mean transition times between O and I states also improves the fit to the amplitude distribution (Fig. 5A, dotted line with triangles). Thus our modeled fluorescence signal suggests that the larger number of channel re-openings causes the number of larger amplitude puffs to increase (Fig. 5A, solid line with filled squares). Note that the higher transition rates between O and I states used here to improve the fits only point to a possibility in SH-SY5Y cells and are not based on single-channel observations. Since we do not have single channel estimates of transition rates in SH-SY5Y cells, we use the values obtained from Sf9 cells in the remainder of the paper.

Baylor and Hollingworth demonstrated that treating ATP as a buffer is important for Ca^{2+} spread within a half sarcomere of a frog skeletal muscle fiber activated by an action potential [29]. They showed that high concentration of ATP elongates the time course of SR Ca^{2+} release transients. In order to quantify the role of ATP buffering in puff dynamics, we repeated our simulation in the presence of ATP as Ca^{2+} buffer. We found that moderate ATP concentration doesn't affect the statistics of elementary Ca^{2+} release events significantly (Fig. 4S). In the Baylor and Hollingworth's model, the peak Ca^{2+} concentration was less than 20 μM. In our case, Ca^{2+} concentration at the channel throat rises as high as 300 μM [30]. We believe that the role of ATP buffering in modulating channel gating kinetics in our model is insignificant due to the high Ca^{2+} concentration at the channel location.

4.2 Puff Termination

Our hypothesis is that puffs terminate because of the self-inhibition of IP_3R channels. To test this hypothesis, we reduced the probability of IP_3R to go inhibited by increasing the mean transition time from state **O** to **I** by a factor f. We changed the reverse mean time by the same factor in order to maintain detailed balance. As we increase the mean transition times between **O** and **I** states the termination times distribution of puffs with $5 \le$ amplitude ≤ 10 shifts to the right showing that reducing the probability of the channel to go inhibited indeed delays the puff termination (Fig. 6A).

There is considerable evidence in cardiac muscles that the local depletion of Sarcoplasmic Reticulum (SR) is the dominant mechanism for sparks termination (see for example [31], and [32] for review). To investigate the **ER** local Ca^{2+} depletion as a possible source for puff termination, we modified the equation for flux through the channel (J_j, see Supplemental Methods) so that it is proportional to the Ca^{2+} gradient across the **ER** membrane, i.e.

$$J_j = \begin{cases} V_f \times (C_{ER} - C) & \text{for } r \le \Delta r, \\ 0 & \text{for } r > 0. \end{cases} \qquad (8)$$

We used flux velocity, $V_f = 1.75 \times 10^4/(\mu\text{Mms})$, so that the current through the channel under optimal conditions (C = 2 μM) is 0.075 pA.

We computed the instantaneous value of Ca_{ER} during the puff by translating the flux through the cluster into the Ca^{2+} concentration loss in a hemisphere of 700 nm radius in **ER** under the cluster. We considered the extreme situation where there is no replenishing of the **ER** micro-domain through Ca^{2+} diffusion or pump. A single channel having current $I = X$ pA releases $N_i = 3125 \times X$ ions/ms. So the total number of ions, N_t, released by the cluster during time Δt is $N_t = N_i \times N_O \times \Delta t$, where N_O is the number of open channels in the cluster at a given time. We integrated N_t from 0 to t for the total number of ions released by the cluster at time t during the puff which started at time 0. One Ca^{2+} ion is equivalent to 1.66 × 10^6 μM × nm^3. Ca^{2+} concentration lost by the hemisphere having volume δV_{ER} in the **ER** during time Δt is $C_{ER}^{lost}=N_t \times (1.66 \times 10^6\ \mu M \times nm^3)/\delta\ V_{ER}$. Thus the instantaneous Ca^{2+} concentration in the **ER** micro-domain is $C_{ER}=C_{ER}^{rest} - C_{ER}^{lost}$. Where C_{ER}^{rest} is the Ca^{2+} concentration in the **ER** at rest.

In Fig. 6B, we show the distribution of puff termination times for three different C_{ER}^{rest} values. We consider puffs with 5 ≤ amplitude ≤ 10 because bigger puffs are more likely to deplete the ER as compared to the smaller puffs with amplitude < 5 (see Fig. 5S). In line with the observations in Fig. 5S, the probability of ER depletion increases as the number of channels in the cluster increases (Fig. 6S). This happens because bigger clusters having more than 10 channels produce larger puffs (amplitude > 10). The total number of puffs with amplitude ≥ 5 also increases as the number of channels per cluster increases. It is interesting to note that the distribution shifts to the left as we increase C_{ER}^{rest} although the probability of local **ER** depletion decreases. For $C_{ER}^{rest}=700\mu M$, one fourth of events cause local **ER** depletion (Fig. 6C, solid line) but the distribution has smaller number of short and larger number of long termination times as compared to $C_{ER}^{rest}=1300\mu M$ where there are no local depletions. Based on this result we rule out local **ER** depletion as a reason for puff termination. Previous experimental observations support our conclusion. First, it is possible to evoke a second puff almost immediately after the first one. The amplitude of the second puff is not correlated with that of the first and on average is no smaller (Fig. 6 of [33]). Second, the stepwise decrements of Ca^{2+} fluorescence as individual channels close during a puff do not get progressively smaller and larger puffs do not terminate faster than smaller puffs [5]. Third, we recently found some instances where puffs fail to terminate. After producing several normal puffs, a puff at a site just keeps going, with a sustained fluorescence amplitude that declines little over several seconds (unpublished data). This last observation is in accord with our result. Had we allowed slow replenishing of **ER** by pump, diffusion, and buffers in case of $C_{ER}^{rest}=700\ \mu M$, the C_{ER} would have a sustained smaller value causing a smaller flux through the channel. The smaller flux would have caused delayed channel inhibition and hence elongated puffs.

5 Discussion

Ca^{2+} ions encode information through their spatiotemporal patters. Puffs and blips are the building blocks of Ca^{2+} patterning. The dynamics of puffs, especially their termination mechanism remain incompletely understood. Here we used data-driven modeling to unveil one mechanism of puff termination. We first developed a single channel model for IP_3R. We assumed that the channel gating kinetics as observed in patch clamp recordings obey the laws of mass action and detailed balance. These two laws together imply that the equilibrium open probability is given by a rational function in terms of the concentrations of the ligands that bind to the channel. Some of the key patch clamp measurements were taken at IP_3= $10\mu M$.

We constrained the model based on key experimental observations regarding single channel gating rather than using existing models. Our model suggests that during a puff, IP_3R channels in a cluster proceed along a one-way trip around a loop through kinetic states from “rest” to “active and open” to “inhibited” and back to “rest” (Fig. 7S). The channels can switch back and forth between active and open states during the puff. However, the puff is terminated by channels entering the inhibited state. There are no channels in the active state immediately after a puff is terminated. In line with experimental observations, we ruled out local **ER** Ca^{2+} depletion as a reason for puff termination unlike Ca^{2+} sparks in cardiac muscles where local SR depletion is the dominant mechanism for spark termination [31, 32]. In the following, we argue further that puffs are terminated by self-inhibition of IP_3Rs.

The problem of understanding puff dynamics is fundamentally a problem of analyzing the various space and time scales in light of the various reaction rates. From the open probability data we note that the occupancy probability for the inhibited state, $P_{\mathbf{I}}$, occurs only at Ca^{2+} concentrations above 10 μM [21]. For the SF9 cells, $P_{\mathbf{I}}$ reaches the ten percent level at $Ca^{2+} = 3.5\ \mu M$ [23] while for *Xenopus Laevis* oocytes the ten percent level is reached only at $Ca^{2+} = 36\ \mu M$ [21]. A key question is whether an open channel can inhibit its neighbor. If we neglect buffers for the moment, and treat an IP_3R as an ideal point source located in a planar membrane, an open channel contributes $I/[2\pi rD]$ to the Ca^{2+} concentration a distance r away where D is the diffusion coefficient of free Ca^{2+} and is in the range of $D \approx .2 - .3\ \mu m^2/ms$. With a mean spacing to nearest neighbor of about 120 nm and $I = 0.075\ pA$, this corresponds to a contribution of about 1.3 – 2.0 μM to the Ca^{2+} that a channel experiences because a neighbor is open. The presence of buffers reduces the contribution so that an open channel contributes $I\ exp(-r/\lambda)/2\pi r\ D$ to Ca^{2+} concentration a distance r away, where λ accounts for the decrease in Ca^{2+} due to Ca^{2+} buffers.

$\lambda = \sqrt{D/(k_{on} B_T)}$ [34]. With total buffer concentration $B_T \approx 100\ \mu M$ [35] and an on-rate, k_s^f of about .2 $\mu M^{-1}\ ms^{-1}$ [36], it is interesting to note that $\lambda \approx 120 nm$, the same as the nearest neighbor spacing. Under such buffering conditions, an open channel contributes 0.5–0.7 μM to the concentration that its average nearest neighbor experiences. P_{O} for both *Xenopus Laevis* and *SF*9 is above the 90% level at 0.7 μM. $P_{\mathbf{I}}$ is zero at 0.7 μM for both *Xenopus* and Sf9. Thus, open channels cannot raise the Ca^{2+} concentration experienced by their neighbors enough to result in significant $P_{\mathbf{I}}$. If channels are to reach the inhibited state, then it must be because they are sensing their own self-contribution to Ca^{2+}.

The IP_3R "outer radius" is about 10nm from the pore. The self-contribution to the concentration at the outer radius is 20 – 40 μM for an open channel and near zero when the channel is closed. Note that when a channel opens or closes, the initial change in concentration very close to the pore is instantaneous. Even at the nearest neighbor distance (~ 120 nm), the time for the concentration field to approach its quasi steady value is about 50 μs, which is very short relative to the channel gating times that are on the order of milliseconds or longer. Upon closing, a channel's self-contribution to the Ca^{2+} concentration it senses at the outer radius drops from 20 – 40 μM to a very small value, depending on buffer, in times of about a microsecond. It follows that the only time that the inhibiting binding site is exposed to concentrations high enough to raise $P_{\mathbf{I}}$ is when the channel is open. Thus, the channel must be open in order to become inhibited. Inhibition means *self-inhibition*. We conclude that the only way for a channel to sense inhibiting levels of Ca^{2+} is if the channel is open, unlike the 9 state model in [37] in which the channel cannot inhibit itself. Thus, puffs terminate because of self-inhibition causing finite puff lifetimes of a few hundred milliseconds.

If we consider n open channels at the peak of the puff that go inhibited independently of each other with τ the mean time to inhibition of a single channel, then the mean time taken by nth, $(n-1)th$, …. , 2nd last, last open channel to close would be τ/n, $\tau/(n-1)$, …., $\tau/2$, $\tau/1$. The total termination time for the puff is $\tau\,(1/n+1/(n-1)+\ldots\ldots+1/2+1)$. As shown in Fig. 5E, the observed mean termination time versus the amplitude of puff nearly follows a harmonic series. The mean termination time for puffs with bigger amplitude given by the model moves away from the harmonic series. After analyzing individual puffs, we noticed that the longer puffs have more re-openings during the falling phase which elongates their termination time. This analysis leads to two conclusions. First, by fitting the puff termination time vs amplitude obtained from experimental data to the harmonic series one can estimate the mean open time of a single channel in a physiological environment. Second, the number of re-openings during the falling phase of the puff increases as we decrease the current through a single channel and vice versa. By using a single-channel Ca^{2+} current $I = 0.02$ pA, we estimated that the channel experience about 75 μM Ca^{2+} when open and the mean termination time for bigger puffs was about 4 times longer than the experimental values. Furthermore, the increased termination time was due to the increased number of re-openings during the falling phase of the puff. To get close to the experimentally observed termination time, we had to increase the channel current to 0.075 pA. Second, the number of re-openings also decreases as we increase the transition rate from state **O** to **I**. Since the mean transition times are constrained by the patch clamp data, we changed the channel current. Thus by fitting the model to the experimental termination time vs amplitude, the current through a single channel can be estimated. A single channel current of 0.075 pA gave us a reasonable fit to the data. This value is well within the observed limits [18-20]. The same practice also enabled us to estimate the Ca^{2+} concentration experienced by the channel due to its opening. Our model predicts that the Ca^{2+} concentration near an open channel can reach 300 μM [30].

We have assumed fixed IP_3 concentration for the puff simulations in this paper. The goal was to understand key observations about puffs in terms of Ca^{2+} dependence only and to investigate the puff termination mechanism. Previous observations indicate that some key characteristics of puffs such as their amplitude are relatively insensitive to IP_3 concentration [38, 39]. Further, we noticed that at 10 μM IP_3 the four state single channel model used for puffs behaves in the same manner as the seven state model that considers explicit IP_3 binding (Supplemental Methods section 1.1). We believe that our conclusion regarding self-inhibition as the mechanism for puff termination remains unchanged even if IP_3 binding is taken into account. The effects of IP_3 binding on IP_3R gating have not been experimentally explored sufficiently to draw firm data-driven conclusions. We are currently investigating the effects of IP_3 binding on the IP_3R channel gating and will report our results in the future.

Supplementary Material

Refer to Web version on PubMed Central for supplementary material.

Acknowledgments

This material is based upon work supported by NIH under grant 5RO1GM065830-08.

References

1. Cheng H, Lederer WJ. Ca^{2+} Sparks. Physiol Rev. 2008; 88:1491–1545. [PubMed: 18923188]
2. Shuai J, Rose H, Parker I. The number and spatial distribution of IP_3Rs underlying Ca^{2+} puffs in Xenopus oocytes. Biophys J. 2006; 91:4033–4044. [PubMed: 16980372]
3. Smith I, Wiltgen S, Shuai J, Parker I. Ca^{2+} puffs originate from pre-established stable clusters of IP_3Rs. Sci Signaling. 2009; 2:1–8.
4. Rahman T, Skupin A, Falcke M, Taylor C. Clustering of IP_3Rs by IP_3 retunes their regulation by IP_3 and Ca^{2+} Nature. 2009; 458:655–659. [PubMed: 19348050]
5. Smith IF, Parker I. Imaging the quantal substructure of single IP_3R channel activity during Ca^{2+} puffs in intact mammalian cells. Proc Natl Acad Sci USA. 2009; 106:6404–6409. [PubMed: 19332787]
6. Callamaras N, Marchant J, Sun X, Parker I. Activation and co-ordination of IP_3-mediated elementary Ca^{2+} events during global Ca^{2+} signals in Xenopus oocytes. J Physiol. 1998; 509:81–91. [PubMed: 9547383]

7. Sun X, Callamaras N, Marchant J, Parker I. A continuum of IP_3-mediated elementary Ca^{2+} signalling events in Xenopus oocytes. J Physiol. 1998; 509:67–80. [PubMed: 9547382]
8. Shuai J, Jung P. Stochastic properties of Ca^{2+} release of IP_3R clusters. Biophys J. 2002; 83:87–97. [PubMed: 12080102]
9. Ullah G, Jung P. Modeling the statistics of elementary Ca^{2+} release events. Biophys J. 2006; 90:3485–3495. [PubMed: 16513779]
10. Shuai J, Pearson J, Parker I. Modeling Ca^{2+} feedback on a single IP_3R and its modulation by Ca^{2+} buffers. Biophys J. 2008; 95:3738–3752. [PubMed: 18641077]
11. Swaminathan D, Ullah G, Jung P. A simple sequential-binding model for Ca^{2+} puffs. Chaos. 2009; 19:037109. [PubMed: 19792034]
12. Rüdiger S, Shuai JW, Sokolov IM. Law of Mass Action, Detailed Balance, and the Modeling of Ca^{2+} Puffs. Phys Rev Lett. 2010; 105:048103. [PubMed: 20867887]
13. Ullah G, Jung P, Machaca K. Modeling Ca^{2+} signaling differentiation during oocyte maturation. Cell Calcium. 2007; 42:556–564. [PubMed: 17349690]
14. Dawson A, Lea E, Irvine R. Kinetic model of the IP_3R that shows both steady-state and quantal patterns of Ca^{2+} release from intracellular stores. Biochem J. 2003; 370:621. [PubMed: 12479792]
15. Solovey G, Dawson S, Chirico G. Intra-cluster percolation of Ca^{2+} signals. PloS one. 2010; 5:e8997. [PubMed: 20174630]
16. Swillens S, Dupont G, Combettes L, Champeil P. From Ca^{2+} blips to Ca^{2+} puffs: theoretical analysis of the requirements for interchannel communication. Proc Natl Acad Sci USA. 1999; 96:13750–13755. [PubMed: 10570144]
17. Parker I, Smith I. Recording single-channel activity of IP_3Rs in intact cells with a microscope, not a patch clamp. J Gen Physiol. 2010; 136:119–127. [PubMed: 20660654]
18. Bruno L, Solovey G, Ventura A, Dargan S, Dawson S. Quantifying Ca^{2+} fluxes underlying Ca^{2+} puffs in xenopus laevis oocytes. Cell Calcium. 2010; 47:273–286. [PubMed: 20097419]
19. Shuai J, Parker I. Optical single-channel recording by imaging Ca^{2+} flux through individual ion channels: theoretical considerations and limits to resolution. Cell Calcium. 2005; 37:283–299. [PubMed: 15755490]
20. Vais H, Foskett KJ, Mak DOD. Unitary Ca^{2+} current through recombinant type 3 IP_3 receptor channels under physiological ionic conditions. 2010; 136:687–700.
21. Mak DOD, McBride S, Foskett KJ. IP_3 activation of IP_3R Ca^{2+} channel by ligand tuning of Ca^{2+} inhibition. Proc Natl Acad Sci USA. 1998; 95:15821–15825. [PubMed: 9861054]
22. Mak DOD, McBride S, Foskett KJ. Spontaneous channel activity of the IP_3R. Application of allosteric modeling to Ca^{2+} and IP_3 regulation of IP_3R single-channel gating. J Gen Physiol. 2003; 122:583–603. [PubMed: 14581584]
23. Mak DOD, Pearson JE, Cheung KH, Datta S, Fernandez-Mongil M, Foskett KJ. Rapid ligand-regulated gating kinetics of single IP_3R Ca^{2+} release channels. EMBO Reports. 2007; 8:1044–1051. [PubMed: 17932510]
24. Sneyd J, Dufour J. A dynamic model of the type-2 IP_3R. Proc Natl Acad Sci USA. 2002; 99:2398. [PubMed: 11842185]
25. De Young G, Keizer J. A single-pool IP_3R-based model for agonist-stimulated oscillations in Ca^{2+} concentration. Proc Natl Acad Sci USA. 1992; 89:9895. [PubMed: 1329108]
26. Schwarz G. Estimating the dimension of a model. The Annals of Statistics. 1978; 6:461–464.
27. Nguyen V, Mathias R, Smith G. A stochastic automata network descriptor for Markov chain models of instantaneously coupled intracellular Ca^{2+} channels. Bull Math Biol. 2005; 67:393–432. [PubMed: 15820736]
28. Neher E. Vesicle pools and Ca^{2+} microdomains: New tools for understanding their roles in neurotransmitter release. Neuron. 1998; 20:389–399. [PubMed: 9539117]
29. Baylor S, Hollingworth S. Model of sarcomeric Ca^{2+} movements, including ATP Ca^{2+} binding and diffusion, during activation of frog skeletal muscle. J Gen Physiol. 1998; 112:297. [PubMed: 9725890]
30. Thul R, Falcke M. Release currents of IP_3 receptor channel clusters and concentration profiles. Biophys J. 2004; 86:2660–2673. [PubMed: 15111387]

31. Zima A, Picht E, Bers D, Blatter L. Termination of cardiac Ca^{2+} sparks: role of intra-SR Ca^{2+}, release flux, and intra-SR Ca^{2+} diffusion. Circulation Res. 2008; 103:e105. [PubMed: 18787194]
32. Rios E, Launikonis B, Royer L, Brum G, Zhou J. The elusive role of store depletion in the control of intracellular Ca^{2+} release. J Muscle Res Cell Motility. 2006; 27:337–350.
33. Callamaras N, Parker I. Phasic characteristic of elementary Ca^{2+} release sites underlies quantal responses to IP_3. The EMBO J. 2000; 19:3608–3617.
34. Smith G. Analytical steady-state solution to the rapid buffering approximation near an open Ca^{2+} channel. Biophys J. 1996; 71:3064–3072. [PubMed: 8968577]
35. Falcke M. Reading the patterns in living cells-the physics of Ca^{2+} signaling. Adv Phy. 2004; 53:255–440.
36. Neher E, Augustine G. Ca^{2+} gradients and buffers in bovine chromaffin cells. J Physiol. 1992; 450:273–301. [PubMed: 1331424]
37. Shuai J, Pearson J, Foskett KJ, Mak DOD, Parker I. A kinetic model of single and clustered IP_3 receptors in the absence of Ca^{2+} feedback. Biophys J. 2007; 93:1151–1162. [PubMed: 17526578]
38. Smith I, Wiltgen S, Parker I. Localization of puff sites adjacent to the plasma membrane: functional and spatial characterization of Ca^{2+} signaling in SH-SY5Y cells utilizing membrane-permeant caged IP_3. Cell Calcium. 2009; 45:65–76. [PubMed: 18639334]
39. Yao Y, Choi J, Parker I. Quantal puffs of intracellular Ca^{2+} evoked by IP_3 in Xenopus oocytes. J Physiol. 1995; 482:533. [PubMed: 7738847]

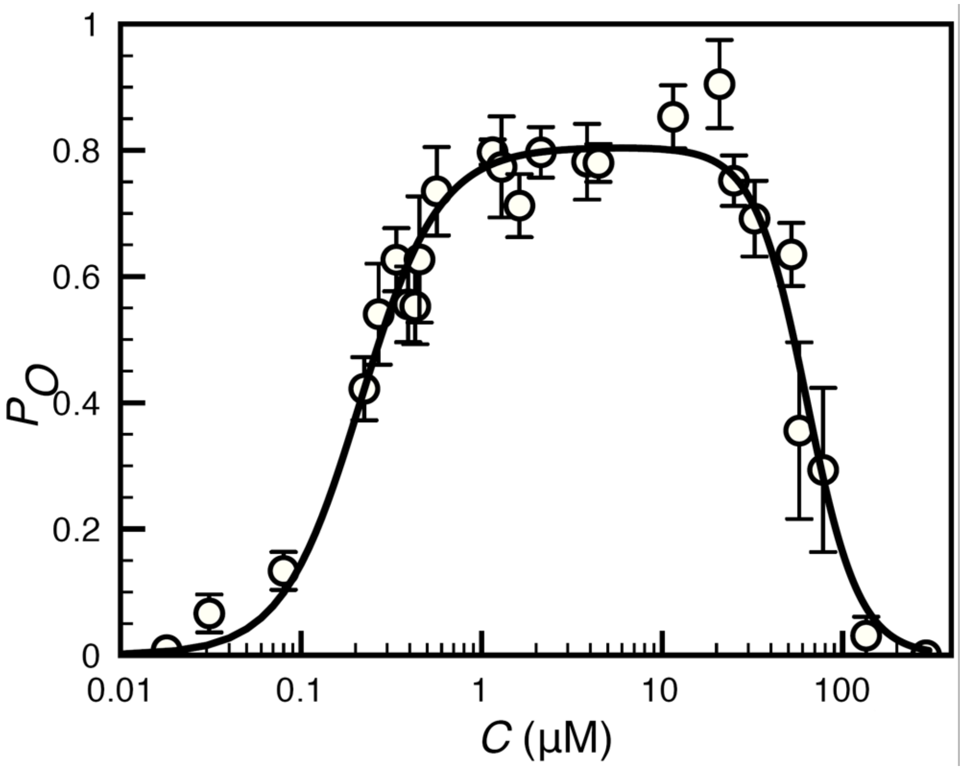

Fig. 1.

Equilibrium open probability of the single IP_3R channel as a function of C at IP_3 concentration of 10 μM. The solid line and circles represent the model fit and the mean P_O from patch clamp experiments on *Xenopus Laevis* occytes [21] respectively. Error bars represent standard errors of the mean.

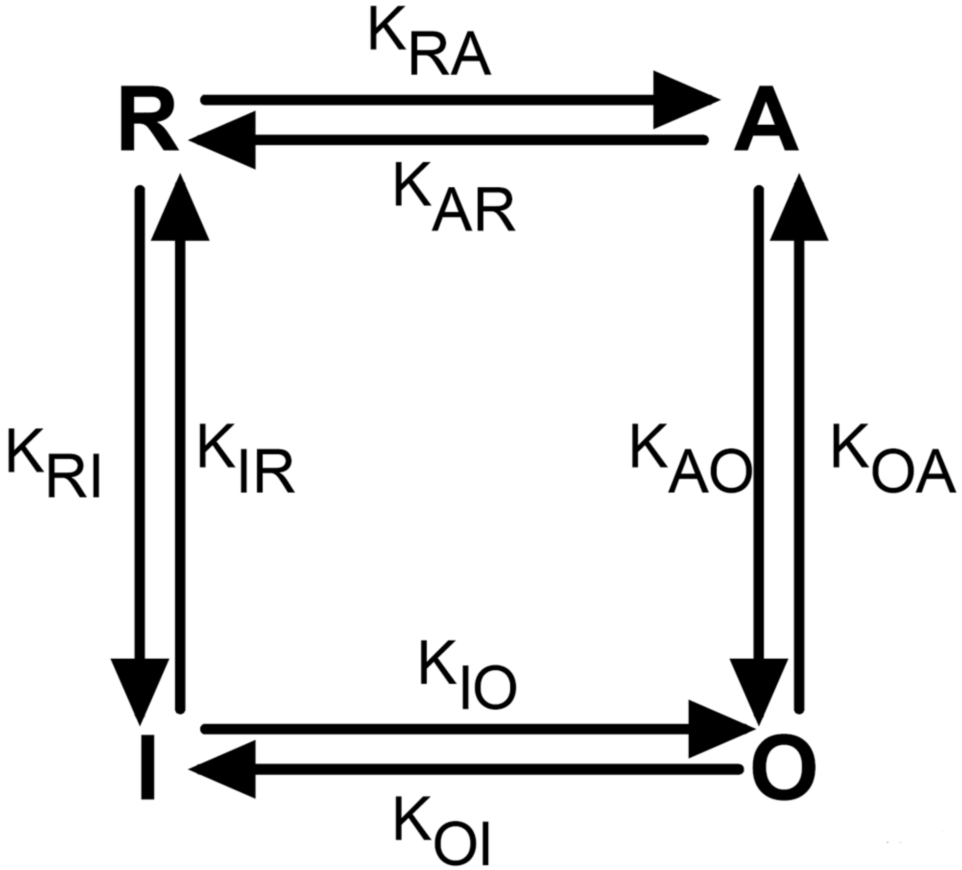

Fig. 2.

Schematic of the four state model for single IP_3R channel. K_{ij} represents the transition rate from state *i* to *j* where *i, j* =**R, A, O, I**.

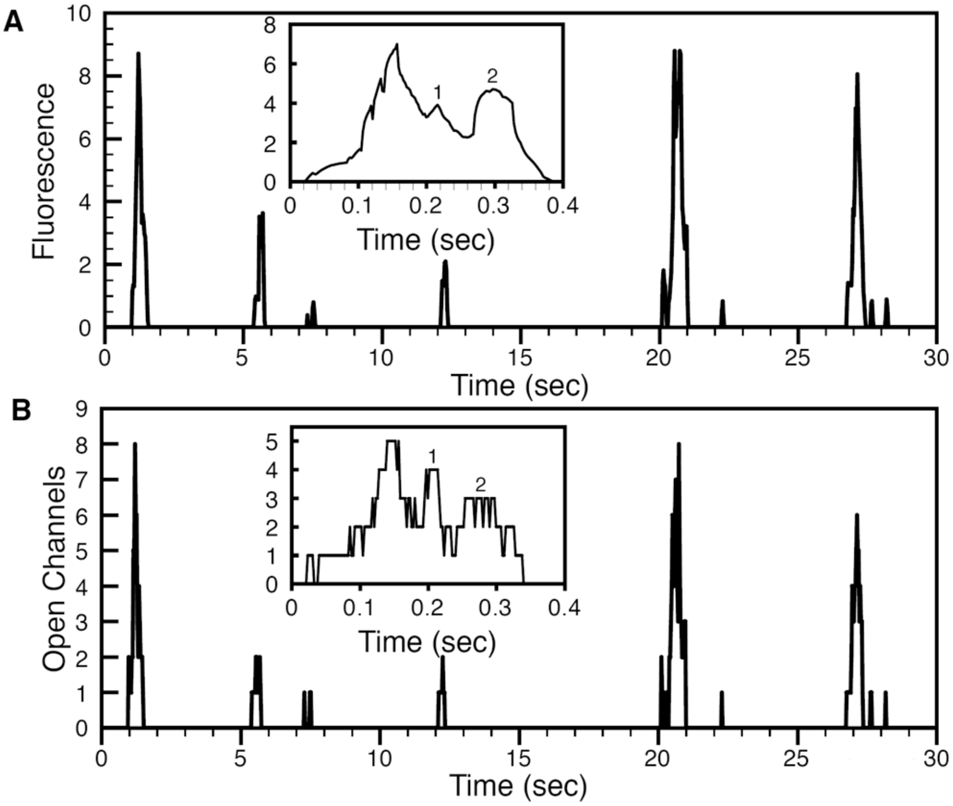

Fig. 3.

Random blips as openings of single channels and puffs as cooperative openings of multiple channels. Change in modeled fluorescence as a result of channel openings and closings in unit of average fluorescence change due to single channel events (i.e. fluorescence changes during thousands of blips were averaged and used as unit for the fluorescence change during puffs) (A) and the corresponding number of channel openings during puffs (B). The insets in (A) and (B) show an expanded view of the same puff.

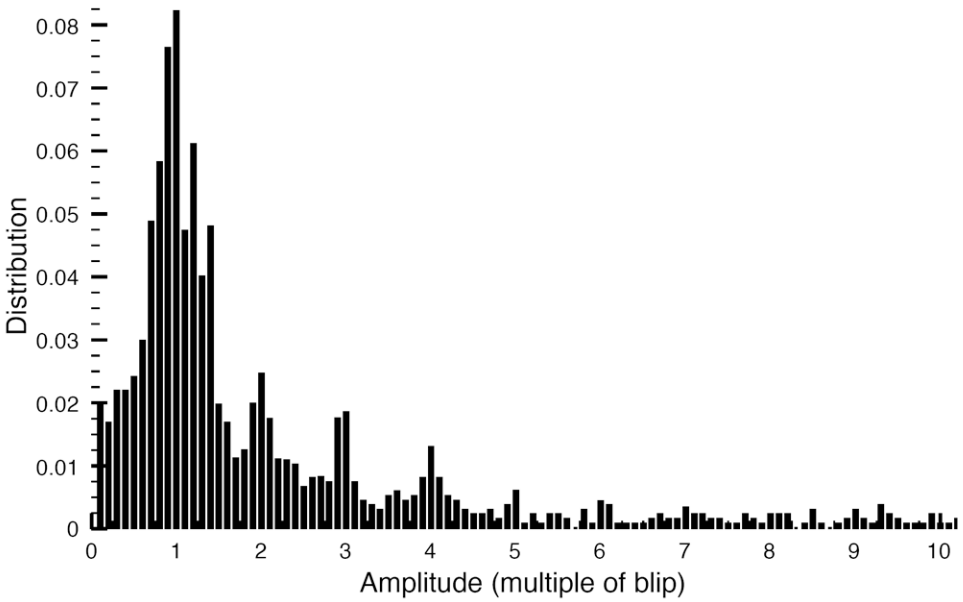

Fig. 4.

Distribution of simulated fluorescence changes due to channel openings during the puff in units of unitary Ca^{2+} events (averaged fluorescence change during blips).

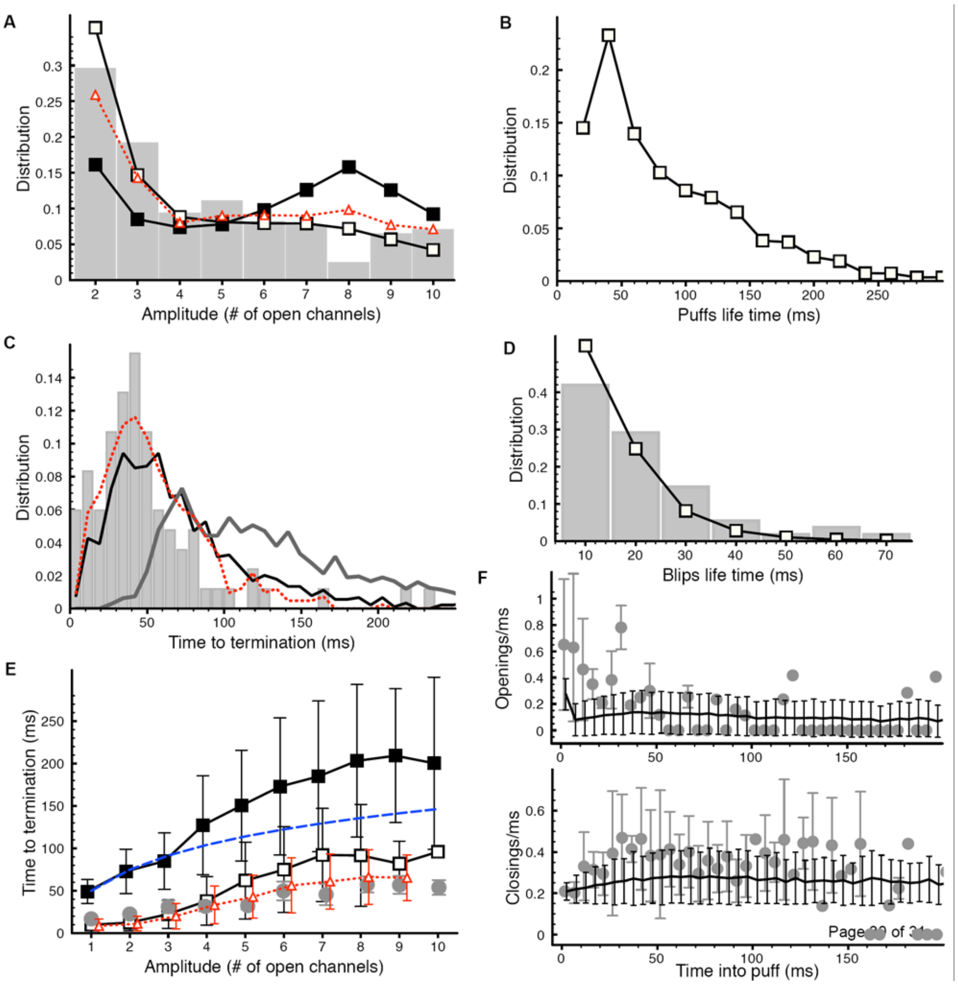

Fig. 5.

Statistics of Ca^{2+} puffs and blips: (A) Distribution of puff peak amplitude obtained from open channels (solid line with open squares), modeled fluorescence (solid line with filled squares), and experimental data (gray bars). The dotted line with triangles is the distribution obtained from modeled fluorescence when mean time for **O** to **I** and **I** to **O** transitions is decreased from 290 ms to 230 ms and 2.4 s to 1.92 s respectively. (B) Puff life time distribution. (C) Distribution of puff termination time obtained from open channels (black line), modeled fluorescence (dark gray line), and experimental data (gray bars). The dotted line represents the distribution obtained from the modeled fluorescence when mean times of 230 ms and 1.92 s are used for **O** to **I** and **I** to **O** transitions respectively. (D) Life time distribution for blips from simulations (solid line with squares) and experiment (gray bars). (E) Mean termination time of puffs as a function of amplitude estimated from open channels (solid line with open squares) and modeled fluorescence (solid line with filled squares). The light gray bullets are the experimental data and dashed line is harmonic series with $n = 10$ and $\tau = 50$ ms. The dotted line with triangles is the model result when mean times of 230 ms and 1.92 s are used for **O** to **I** and **I** to **O** transitions respectively. (F) The number of openings/ms (upper panel) and closings/ms (lower panel) per puff as a function of time into puff given by the model. In (F) the gray bullets represent the experimentally observed openings/ms (upper panel) and closings/ms (lower panel). Experimental data reproduced from [5] with permission.

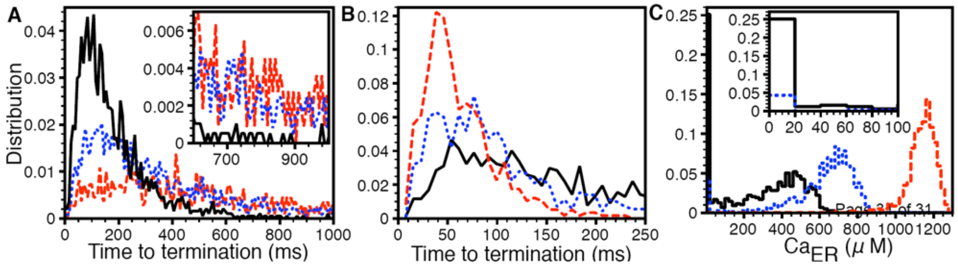

Fig. 6.

Puffs are terminated by IP_3R inhibition not local **ER** depletion. (A) Distribution of time to termination of puffs for $f = 2.5$, 5, and 10 (solid, dotted, and dashed line respectively). The inset is an expanded view from 600 ms to 1000 ms. (B) Termination time distribution for C_{ER}^{rest}=700 μM, 900 μM, and 1300 μM (solid, dotted, and dashed line respectively). (C) Local **ER** Ca^{2+} concentration for simulations in (B). Different line patterns correspond to the same C_{ER}^{rest} values as in (B). The inset is an expanded view from 0 to 100 μM.